Sensors and Environmental Applications of Remote Sensing, Askne (ed.) © 1995 Balkema, Rotterdam, ISBN 90 5410 524 0

Improved forest mapping by combining corrections of atmospheric and topographic effects in Landsat TM imagery

Joachim Hill & Wolfgang Mehl
Institute for Remote Sensing Applications, Environmental Mapping and Modelling Unit, Commission of the European Communities, Joint Research Centre, Ispra (Va), Italy

Volker Radeloff
Remote Sensing Department, Faculty of Geography/Geosciences, University of Trier, Germany

ABSTRACT. The spectral reflectance of ground objects in mountainous areas is largely contaminated by second order effects which are due to topographic slope and aspect. Such topographic effects present severe problem for the consistent analysis of optical remote sensing images, in particular for satellite-based forest cover mapping. We have integrated a topographic correction module into a modified 5S atmospheric correction model, where targets are assumed to have lambertian reflectance characteristics. The method was successfully applied to four Landsat Thematic Mapper images with large seasonal differences in solar elevation. Classification methods of increasing complexity (euclidian minimum distance, maximum likelihood, and a backpropagation neural network) have then been used to produce forest stand maps from images which were either corrected for atmospheric effects only or for radiometric distortions due to both atmosphere and topography. It is demonstrated that the topographic corrections provide important improvements when direct and diffuse radiation components are properly accounted for. Differences between the actual bidirectional reflectance properties of forest stands and their approximation by Lambertian reflectance characteristics seem to be less important.

1 INTRODUCTION

It is commonly known that the spectral reflectance of ground objects in mountainous areas is largely contaminated by second order effects which are due to topographic slope and aspect. Particularly in remote sensing images acquired over homogeneous ground cover, reflectance variations due to the topographic effect are perceived as a visual impression of relief. Slopes facing away from the sun appear relatively dark, while the sun-facing slopes appear brighter than horizontally oriented surfaces with the same cover type. It is evident that this effect varies throughout the year as a function of sun elevation and azimuth, and the steepness and orientation of slopes. In extreme cases, effects of self shadowing and shadows cast on opposite slopes may occur frequently, causing further disturbances in the radiometric consistency of satellite images.

The topographic effect presents a severe problem for any consistent analysis of optical remote sensing images, in particular for automated land cover classification (Hill, 1993). This affects especially the production of precise satellite maps over forested areas which tend to be dominant in mountainous areas, being less suitable for other land uses.

The principles of terrain illumination have been described in detail, and various approaches for topographic correction or normalisation were already presented (Justice et al., 1981; Dozier and Frew, 1981; Woodham and Gray, 1987; Leprieur et al., 1988; Kawata et al., 1988; Civco, 1989; Proy et al., 1989; Colby, 1991; Itten et al., 1992; Conese et al., 1993). The most critical issue in correcting the topographic effect seems related to selecting a suitable bidirectional reflectance distribution function (BRDF) for determining how a surface will appear under any condition of viewing. Using the BRDF of a Lambertian reflector and a class of reflectors first identified by Minnaert (1941) have provided partially contradictory results, such that it has recently been recommended to identify empirical correction factors by a regression analysis of the relationship between terrain slope/aspect and corresponding pixel intensities from forested areas (Itten et al., 1992).

We have attempted to integrate the correction of the topographic effect into our implementation of the 5S atmospheric correction model of Tanré et al. (1990). In order to study whether frequently reported shortcomings of topographic corrections (usually attributed to deficient approximations of the surface BRDF) might also be due to improperly balanced direct and diffuse solar radiation terms, our topographic correction was initially implemented under the assumption of Lambertian reflectance characteristics.

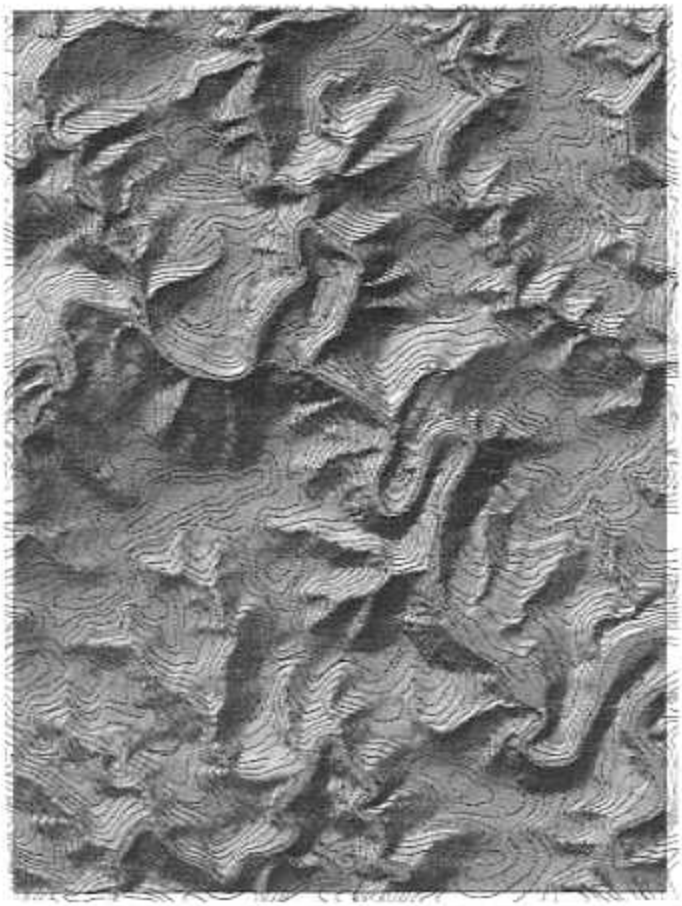

Figure 1. Digital elevation model of the Heiderscheid study area, illuminated according to the conditions during the Landsat satellite overpass from 21 September 1989 (top of page is north). Colour plate see page 492

2 STUDY SITE

This study is embedded in a more extensive experiment on automatic updating of the CORINE Land Cover data base on the Grand-Duchy of Luxembourg where we have used multi-temporal Landsat Thematic Mapper data from 1989. Ground reference mapping was obtained within 105 segments (50 ha) during summer 1991 in cooperation with the "Direction des Eaux et Forêts", the "Institut Supérieur de Technologie" (Luxembourg) and the Remote Sensing Department of the University of Trier (Germany). Due to the fact that the reference data were collected 2 years later than the satellite imagery, only the forest-related ground data could be used to directly assess the accuracy of the mapping results. Although an overall precision of 78 % was achieved for the satellite-based mapping of deciduous and coniferous forest stands, this accuracy may locally drop to lower values, particularly in areas of rugged terrain with strong illumination differences.

A smaller study site was selected for analysing possibilities of improving forest mapping accuracy through a correction of the topographic effect in the satellite images. This site covers an area of 52.9 km^2 and is located in the Oesling region of Luxembourg (Ardennes foothills), north-west of the towns Diekirch and Ettelbruck. Although the maximum altitude is only 512 m above sea level, the Heiderscheid test area is characterised by deeply incised, meandering valleys with pronounced illumination differences (figure 1).

In particular the steep slopes of the V-shaped valleys are mostly covered with forests, where coppice-like *Niederwälder* of oaks are dominant. Climax vegetation would be dominated by mixed beech (fagus silvatica) and oak (quercus robur) forests. Since the early 18th century, fir (abies alba) was introduced, and afforestations with various coniferous species have become popular ever since.

Table 1. Cloud-free Landsat-5 Thematic Mapper images in 1989 (Path 197, Row 25)

Date	Acquisition time (GMT)	Scene centre latitude	Scene centre longitude	Sun elevation	Sun azimuth
16 May 1989	9:56.33	50.28° N	5.93° E	53.47°	139.76°
17 June 1989	9:55.54	50.28° N	5.94° E	56.37°	134.45°
20 Aug 1989	9:54.39	50.28° N	5.92° E	46.44°	141.16°
21 Sep 1989	9:53.47	50.28° N	5.94° E	36.35°	149.82°
10 Dec 1989	9:52.42	50.28° N	5.91° E	13.67°	156.97°

3 DATA SETS

Detailed forestry information for the Heiderscheid study site was obtained from the Luxembourg "Direction des Eaux et Forêts", and has been introduced into a georeferenced data base under ARC-Info and ORACLE. A detailed digital elevation model (elevation, slope, aspect) with a spatial resolution of 10x10 meters was generated from digitised contour lines of the 1:20,000 scale topographic maps, using the ARC-Info TIN module (figure 1).

In 1989 the for central European conditions relatively rare situation occurred that five cloud-free Thematic Mapper scenes were acquired by the Landsat-5 satellite (table 1). All scenes have been system-processed by SSC Satellitbild (Sweden), and were delivered as geocoded products in UTM-projection, being resampled with the cubic convolution scheme. The December image was not used in this study, because the signal dynamics is by far too low.

4 CORRECTING THE TOPOGRAPHIC EFFECT

In case of an inclined surface, the intercepted radiance due to direct solar illumination is proportional to the cosine of the angle γ between local surface normal and the direction of the incoming sunlight

$$\cos(\gamma) = \cos(\theta_0)\cos(\theta_n) + \sin(\theta_0)\sin(\theta_n)\cos(\phi_n - \phi_0), \quad (1)$$

where θ_0 is the solar zenith angle, θ_n the zenith angle of the normal to the surface, ϕ_0 the solar azimuth angle, and ϕ_n the topographic aspect angle. Assuming that the target behaves as a lambertian reflector, also the reflected radiance is proportional to cos (γ) which can be derived for each pixel from registered digital elevation data. Various correction approaches have been proposed most of which attempt to correct the topographic effect through this simple cosine correction, i.e. separately from a correction of atmospheric effects (i.e., Itten et al. 1992).

4.1 *Simple cosine correction*

Assuming lambertian reflectance characteristics, the corrected radiance (which would be observed in case of horizontal orientation) for a pixel on sloping ground is calculated with

$$L_h = L_s \cdot \cos(\theta_0)/\cos(\gamma) \quad (2)$$

where L_h denotes the corrected radiance corresponding to a horizontal surface, and L_s the actually observed radiance over sloping ground; θ_0 is the sun zenith angle (90° - sun elevation angle), and γ refers to the angle between the incident solar radiation and the surface normal on a tilted plane (pixel) which is derived from digital elevation models.

Almost as often as this simple method (cosine correction) has been used, it has also been reported that the approach tends to produce overcorrected images, in particular when the angle between the incoming irradiance and the pixel's surface normal is larger than 55°, implying values for cos (γ) < 0.57 (Civco, 1989; Colby, 1991; Itten et al., 1992). This is usually attributed to the fact that the BRDF of most surface types is not lambertian, and several modifications have been proposed in order to better account for the directional reflectance characteristics of important surface cover types (e.g., Minnaert coefficients, empirically derived correction factors).

However, it must be emphasised that this simple cosine correction applies only to the directly transmitted part of the solar irradiance. Diffuse irradiance terms which, depending on the turbidity of the atmosphere, may be of substantial magnitude are not accounted for correctly. In other words, applying the simple cosine approach (conceptually limited to direct irradiance terms) for correcting an effect which results from the combined direct and diffuse illumination, *must produce* overcorrection phenomena, notwithstanding any assumptions about targets behaving like lambertian reflectors. Corrections of the topographic effect should be directly integrated into atmospheric correction models, because these can provide realistic estimates of direct and diffuse irradiance terms.

4.2 *Topographic corrections as an integral part of atmospheric modelling*

We have therefore tried to incorporate a topographic correction module into a radiative transfer code. The atmospheric correction method is originally based on the formulation of radiative transfer as developed by Tanré et al. (1990), and it was modified to account for atmospheric extinction processes as a function of sensor and terrain altitude (Hill and Sturm, 1991; Hill, 1991). The modified '5S' code makes extensive use of analytical expressions and preselected atmospheric models, resulting in a rather short execution time. It provides corrections for atmospheric absorption, scattering and pixel adjacency effects, where diffusion and absorption processes are assumed to be independent. Upward and downward transmission coefficients are derived by introducing the auxiliary quantity of optical thickness τ which measures the total extinction of a light beam due to molecular and aerosol scattering when passing through an airmass. Multiple scattering is accounted for according to Sobolev's approximate solution (Sobolev, 1963), and absorbing atmospheric gases are assumed to condense at the top of the atmosphere and at the top of the layer between the earth surface and the sensor altitude.
An important element of the code is its ability to estimate atmospheric key parameters, such as the aerosol optical depth, directly from dark objects (e.g., water) in the satellite image (Hill, 1993).

Once the aerosol optical depth τ_a is known* , the downward direct (beam) and diffuse transmittance terms ($t_d\downarrow$, $t_s\downarrow$) for a given wavelength λ are calculated with

$$t_d\downarrow = \exp\left(-(\tau_r + \tau_a)/\mu_0\right) \qquad (3)$$

and

$$t_s\downarrow = \exp\left(-(0.52\cdot\tau_r + 1/6\cdot\tau_a)/\mu_0\right) - t_d\downarrow , \qquad (4)$$

where μ_0 denotes the cosine of the solar zenith angle θ_0 (Tanré et al., 1979). The attenuated global irradiance at ground (E_g) in this spectral bandpass is then obtained as the sum of direct and diffuse irradiance terms

$$E_g = E_0' \cdot t_d\downarrow + E_0' \cdot t_s\downarrow . \qquad (5)$$

E_0' denotes the exoatmospherical solar irradiance E_0, being already corrected for ozone absorption.

Assuming lambertian reflectance characteristics, the satellite-measured radiance L_t for a horizontal surface relates to the modelled target reflectance ρ_t according to

$$L_t = E_g \cdot \rho_t \cdot T\uparrow / \pi . \qquad (6)$$

$T\uparrow$ denotes the total upward transmittance in the spectral band. With all other variables but E_g unchanged, the modelled reflectance for an inclined surface is obtained from

$$\rho_t^* = \frac{L_t \cdot \pi}{E_g^* \cdot T\uparrow} , \qquad (7)$$

where E_g^* denotes the slope-aspect-corrected global irradiance. Substituting L_t in equ. (7) by the right-hand term of equ. (6), we obtain

$$\rho_t^* = E_g \cdot \rho_t / E_g^* , \qquad (8)$$

yielding the illumination-corrected target reflectance ρ_t^*. The objective is therefore to find a good approximation for the direct and diffuse components of E_g^*. In order to do so, we have to examine with greater detail the illumination of mountainous areas where the topography modifies the irradiance in different ways (Proy et al., 1989):

(a) the direct irradiance and also parts of the diffuse radiation are modulated according to the pixel orientation
(b) the topography may also cast shadows on a pixel so that it receives no direct radiation
(c) the topography may reduce the scattered (diffuse) sky radiation by hiding a part of the sky hemisphere
(d) the topography may reflect radiation towards the pixel, thereby providing an additional irradiance source

Neglecting the effect noted under (d), we can state that a pixel receives in

case 1: direct and diffuse radiation when cos (γ) > 0, and no shadow is cast on the pixel by other topographic features
case 2: only diffuse radiation when cos (γ) > 0, but shadow is cast on the pixel by other topographic features
case 3: only diffuse radiation when cos (γ) < 0 , i.e. self shadow.

While in previous work diffuse solar radiation was mostly treated as being isotropic, it has been demonstrated by various authors (e.g., Proy et al., 1989) that it is important to consider its anisotropic distribution. Similar to Conese et al. (1993) we have also used Hay's approximate solution (Hay, 1979; Hay and McKay, 1985; Hay et al., 1986). According to this approach, the diffuse downwelling radiance increases in the circumsolar zone, while it is isotropically distributed for the rest of the sky dome. In Hay's approximation the relative weights of anisotropic and isotropic parts of the diffuse irradiance depend on a wavelength-dependant anisotropy index

$$k = \left(E_0' \cdot t_d\downarrow\right) / E_0 , \qquad (9)$$

* the molecular optical depth τ_r is derived from the classical relation $\tau_r = 0.0088\ \lambda^{(-4.15 + 0.2\ \lambda)}$

which is based on the assumption that "the isotropic and circumsolar components are a linear combination based on the transmissivity of the direct radiation." (Hay et al., 1985). The secondary maximum of diffuse radiation near the horizon which is due to the longer path length (Temps & Coulson, 1977) is neglected in this approximation. It follows from equ. (9) that k also varies with the atmospheric conditions.

Accordingly, the value of E_g* to be used in equ. (8) is calculated either with

$$E_g^* = (E_0' \cdot t_d \downarrow) \cdot \cos(\gamma) / \cos(\theta_0) + (E_0' \cdot t_s \downarrow) \cdot k \cdot \cos(\gamma) / \cos(\theta_0) + (E_0' \cdot t_s \downarrow) \cdot (1-k) \cdot Fr_{sky} \quad (10)$$

(i.e., case 1: the sum of direct, anisotropic diffuse (circumsolar), and isotropic diffuse irradiance), or with

$$E_g^* = (E_0' \cdot t_s \downarrow) \cdot (1-k) \cdot Fr_{sky} \quad (11)$$

(i.e., case 2/3: only isotropic diffuse irradiance). For each pixel, Fr_{sky} quantifies the proportion of the hemispherical sky which is not hidden by topographic features in its surroundings. It is determined through an analysis of the digital elevation model, where the local horizon is calculated for 16 directional segments, starting from north (= 0°) in increments of 22.5°. The addition of these visible sky segments provides a good approximation for the hemispherical sky which contributes to the isotropic diffuse illumination of a pixel.

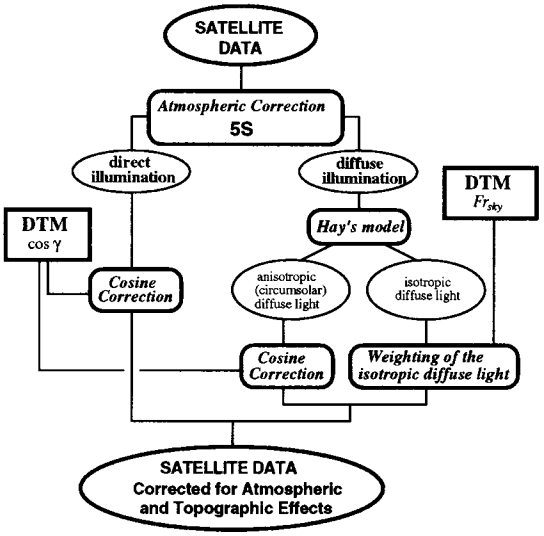

Figure 2. Simplified flow-chart of the processing scheme for combining atmospheric and topographic corrections of satellite imagery.

The flow-chart of Figure 2 summarises this processing scheme for obtaining atmospherically and topographically corrected satellite images, which then will be subject to further thematic analysis.

4.3 *Validation of the topographic corrections*

All Landsat images were processed according to the scheme which was described in the previous section. Atmospheric conditions for each scene were estimated from the satellite-measured radiance over two clear lakes in the vicinity of the Heiderscheid study site (Lac de Haute Sûre, Reservoir de Vianden). The comparison of reference signatures from a horizontal surface with uniform reflectance characteristics (Luxembourg Airport) confirms that these corrections have efficiently reduced the atmosphere-dependant radiometric differences between the images (figure 3).

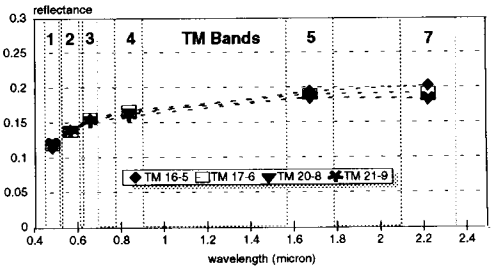

Figure 3. Spectral signatures from a horizontal surface with uniform reflectance characteristics (asphalt, Luxembourg Airport), after atmospheric correction.

Although some noise has been introduced by high frequency terrain features which were present in the digital elevation model, visual examination of the corrected images indicates obvious improvements. Compared to atmospherically corrected images, the additional correction of the topographic effect has substantially reduced the relief-induced illumination differences in all images (figure 4).

A more quantitative validation of the correction method is obtained through a regression analysis of the relationship between cos γ and the modelled scene reflectances for all forest pixels. As anticipated, significant linear relationships are obtained prior to correcting the topographic effect (figure 5). These relationships, the correlation coefficient of which increases with lower sun elevation, collapse after the slope-aspect correction. For all images, the slope of the regression line as well as the correlation between the two variables is then fluctuating around zero, thereby indicating that illumination-dependant variations of pixel intensities have been successfully removed (figures 5, 6).

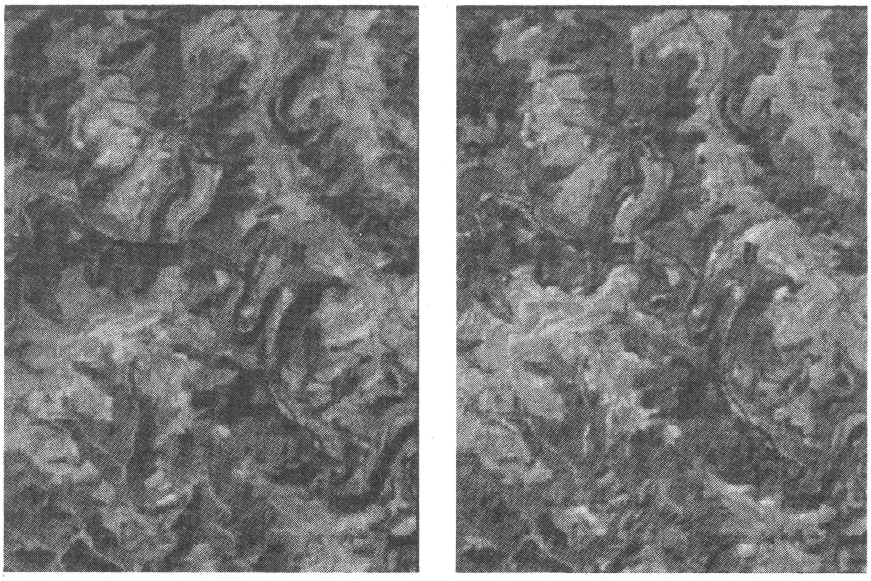

Figure 4. Colour composite of the Landsat image from 20 August 1989 (band combination is 4-5-3 in red-green-blue): atmospheric correction only (left) and atmospheric/topographic correction (right). Colour plate see page 493

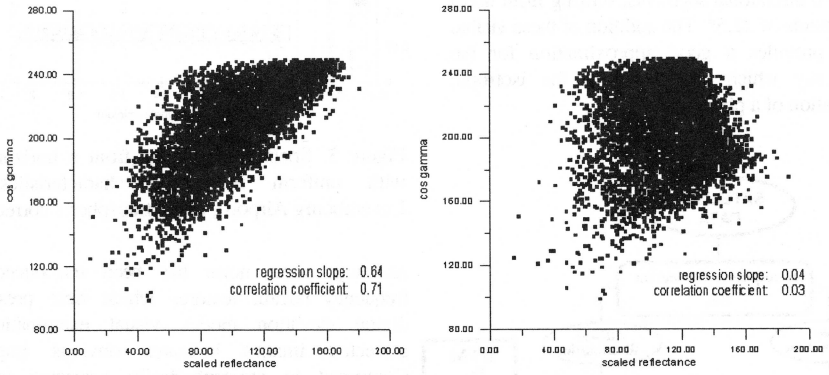

Figure 5. Relationship between cos γ and modelled pixel reflectances in the TM near-infrared spectral band (TM 4), for all forest pixels prior to and after correcting the topographic effect (Landsat TM, 20 August 1989, 9:54 h GMT).

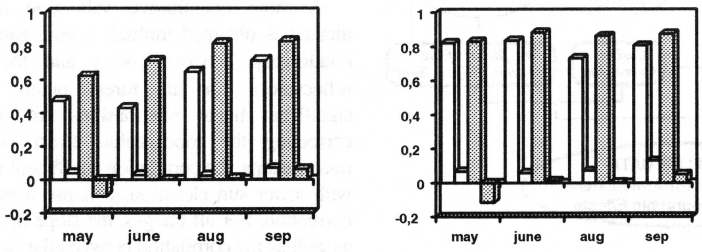

Figure 6. Relationship between cos γ and modelled pixel reflectances in the TM near-infrared spectral band (TM 4) for deciduous (white) and coniferous forest (grey) prior to and after correcting the topographic effect for each acquisition date

Table 2. Percentage of error in mapping deciduous and coniferous forest stands and the relative improvement through the topographic corrections

corrections	May		June		August		September	
	only atmos.	atmos. + topo.	only atmos.	atmos. + topo.	only atmos.	atmos. + topo.	only atmos.	atmos. + topo.
Euclidean Distance	22.4	21.1 (+1.3)	16.2	13.8 (+2.4)	25.9	14.3 (+11.6)	26.3	19.0 (+7.3)
Maximum Likelihood	17.6	11.8 (+5.8)	13.3	14.0 (-0.7)	25.8	14.8 (+11.0)	27.8	19.9 (+7.9)
Neural Network	15.4	11.5 (+3.9)	12.9	12.6 (+0.3)	24.6	14.5 (+10.1)	26.2	19.4 (+6.8)

An examination of the regression slopes is particularly important because these should become negative in case of overcorrecting the topographic effect. This effect, however, occurs only in the May image, which might be related to the high transmissivity of oak leaves during the sprouting period in April/May, and as such correspond to substantial deviations from lambertian reflectance characteristics. For all other dates, no indications of overcorrections are evident which may seriously question the use of lambertian reflectance behaviour as a pragmatic solution for processing optical satellite data over forested areas.

However, severe overcorrection of the topographic effect occurs when the diffuse component of the atmospheric transmittance is not correctly accounted for. This can be demonstrated by comparing a correction with scene-estimated atmospheric parameters and a simulation where the atmosphere is assumed to be unrealistically clear (only molecular, no aerosol scattering). In the latter case, the diffuse radiation component is underestimated by the model such that a too high proportion of the global irradiance is corrected by the cosine correction. This affects in particular the TM bands in the visible part of the spectrum.

It is therefore concluded that an incorrect separation into direct and diffuse radiation components rather than the bidirectional properties of the forest canopy might be the main reason for missing improvements in thematic mapping applications which have been conducted after empirical topographic corrections (i.e., cosine correction).

5 IMPROVEMENTS OF FOREST STAND MAPPING AFTER TOPOGRAPHIC CORRECTIONS

Three classification methods of increasing complexity, such as the classical euclidian minimum distance and maximum likelihood classifiers and a backpropagation neural network (Kanellopoulos et al., 1992), have been used to compare the mapping results obtained from Thematic Mapper images which were either corrected for atmospheric effects only or for both atmospheric and topographic effects. The classification experiment concentrates only on the forested parts of the Heiderscheid study site. All other land cover types have been excluded by applying a corresponding mask which was obtained from the digitised forest stand information of the "Direction des Eaux et Forêts" (see section 3). It is important to mention that an equivalent separation of forested and non forested areas can also be obtained by applying unsupervised classification techniques to the corrected images, thus reducing substantially the omission errors in the uncorrected images (i.e., forested areas on illuminated slopes not mapped as forest but grassland). This already provides an improvement of about 30 % in comparison to the uncorrected images.

Spectral signatures for several forest sub-classes were obtained for each corrected satellite image through unsupervised cluster analysis within the forested areas. The different classifiers have been trained with identical pixel samples, and the mapped sub-classes were then regrouped into deciduous and coniferous stands. About 70 % of the available ground data* have been used to assess the accuracy of the mapping results (table 2).

Our statistical evaluation of the mapping accuracy for the four dates confirms the visual impression of the produced stand maps (figure 7). In addition to the above mentioned reduction of illumination-dependant omission errors, the topographic corrections also provide substantial improvements in the separation between deciduous and coniferous stands, except for the scene from mid June. This was expected because the topographic effect is minimum at this time of the year.

Differences between the various classification methods are small except for the May image. The best results with mapping accuracy close to 90 % are achieved for the images from May (optimum separation between deciduous and coniferous stands during the sprouting period of the deciduous trees), but the results from the June (86 %) and August scenes (85 %) are also acceptable, taking into account the difficult topography and the high fragmentation of the forests. Most improvements are

* forest stands smaller than 3 pixels were discarded.

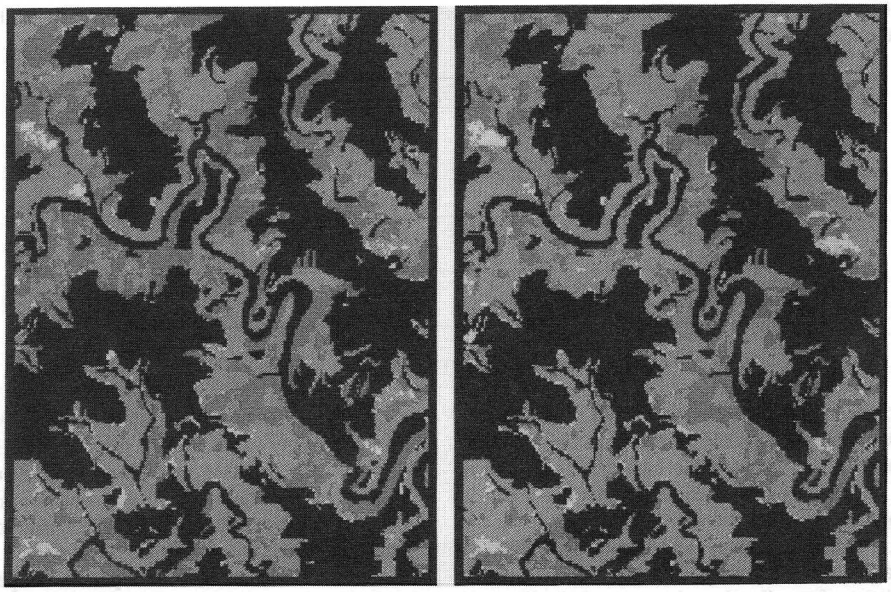

Figure 7. Comparison of forest mapping results for the Landsat TM scene from 20 August 1989, obtained with the neural network classifier before and after topographic corrections (blue - conifers, green - deciduous, yellow - storm damage). Colour plate see page 493

achieved in August and September when the sun elevation is low and leafs are matured.

The remaining errors mainly result from misclassified plantations of young conifers (spectrally not separable from deciduous trees) and from poorly illuminated and shadowed areas which, similar to the results of Kawata et al. (1988), are not fully recovered with our correction method. This explains in particular the reduced mapping accuracy for the September image. It seems that further improvements can only be achieved when the near-horizontal increase of the diffuse irradiance is also accounted for.

These results show that the correction of terrain illumination improves forest mapping also in areas of rugged topography, and it is demonstrated that robust mapping can be achieved when satellite data are pre-processed in an optimum way. None of the classifiers exhibits a particular advantage, except that, for May and June, the maximum likelihood and neural network classifiers perform better than the minimum distance approach. The reasons for this difference are not yet fully understood.

6 CONCLUSIONS

The combination of high quality terrain models, atmospheric and topographic correction modules has shown its suitability to efficiently minimise the effects of illumination differences which are present in optical satellite images of mountainous terrain. Visual examination of the corrected scenes as well as the statistical analysis of mapping results which were obtained with various classification algorithms confirm that reliable separation of deciduous and coniferous stands (accuracy of 85 to 90 %) can be achieved even in highly fragmented forest regions of complex topography.

Separation and correct estimation of direct and diffuse solar radiation components forms the basis for successful corrections of the topographic effect. Differences between the actual bidirectional reflectance properties of forest stands and their approximation by Lambertian reflectance characteristics appeared less important, at least for the Landsat TM scenes which were analysed in this study.

It is concluded that the combination of digital satellite images, topographic data and existing forest information in a GIS-environment opens promising perspectives for operational mapping applications. Further research should be done in other test areas, maybe in alpine regions, in order to understand whether the quality of commercially available DTMs (30 to 50 m resolution) is sufficient for improving forest mapping, so that the method could be applied on larger regions. Whether or not more detailed forest mapping (information on age, density or other ecological parameters) will be possible with such corrections can not be said so far. Finally, the introduction of improved models of the bidirectional behaviour of forest stands could lead to additional improvements.

It is further concluded that optimised radiometric pre-processing of optical satellite imagery is more important for obtaining robust results in forest stand mapping than the use of particular classification approaches.

7 ACKNOWLEDGEMENTS

The authors wish to thank I. Kanellopoulos (JRC) for providing the neural network classifier and his advise, and K. Fullerton (JRC) for her support in using ARC-Info and Oracle. Thanks are also due to the "Direction des Eaux et Forêts" of the Grand-Duchy Luxembourg for providing the forestry information, and to K. Itten and S. Sandmeier (Remote Sensing Laboratories, University of Zurich, Switzerland) for discussions about the topographic corrections.

8 REFERENCES

Civco, D.L., 1989, Topographic normalization of Landsat Thematic Mapper digital imagery, *Photogrammetric Engineering and Remote Sensing*, vol. 55, no. 9, 1303-1309.

Colby, J.D., 1991, Topographic normalization in rugged terrain, *Photogrammetric Engineering and Remote Sensing*, vol. 57, no. 5, 531-537.

Conese, C., M.A. Gilabert, F. Maselli and L Bottai, 1993, Topographic normalization of TM scenes through the use of an atmospheric correction method and digital terrain models, *Photogrammetric Engineering & Remote Sensing*, vol. 59, no. 12, 1745-1753.

Dozier, J. and J. Frew, 1991, Atmospheric corrections to satellite radiometric data over rugged terrain, *Remote Sensing of Environment*, 11, 191-205.

Hay, J.E., 1979, Calculation of monthly mean solar radiation for horizontal and inclined surfaces, *Solar Energy*, vol. 23, 301-307.

Hay, J.E. and D. McKay, 1985, Estimating solar irradiance on inclined surfaces: a review and assessment of methodologies, *Int. J. Solar Energy*, vol. 3, 203-240.

Hay, J.E., R. Perez and D. McKay, 1986, Technical note: Addendum and errata to the paper "Estimating solar irradiance on inclined surfaces: a review and assessment of methodologies", *Int. J. Solar Energy*, vol. 4, 321-324.

Hill, J., and D. Aifadopoulou, 1990, Radiometric comparison of Landsat-5 TM and SPOT HRV-1 sensors for the use in multiple sensor approaches, *Remote Sensing of Environment*, vol. 34, 55-70.

Hill, J. and B. Sturm, 1991, Radiometric correction of multi-temporal Thematic Mapper data for use in agricultural land-cover classification and vegetation monitoring, *Int. J. Remote Sensing*, vol. 12, no. 7, 1471-1491

Hill, J., 1991, Analysis of GER Imaging Spectrometer data acquired during the European Imaging Spectrometry Aircraft Campaign (EISAC '89), *EARSeL Advances in Remote Sensing*, vol. 1, no.1, 64-77.

Hill, J., 1993, *High precision land cover mapping and inventory. The Ardèche Experiment*, EUR 15271, (Office for Official Publications of the European Communities: Luxembourg).

Itten, K.I., P. Meyer, T. Kellenberger, R. Leu, S. Sandmeier, P. Bitter and K. Seidel, 1992, *Correction of the impact of topography and atmosphere on Landsat-TM forest mapping of alpine regions*, Remote Sensing Series, vol. 18, (University of Zurich: Zurich, Switzerland).

Justice, C.O., S.W. Wharton and B.N. Holben, 1981, Application of digital terrain data to quantify and reduce the topographic effect on Landsat data, Int. J. Remote Sensing, 2, 213.

Kanellopoulos, I., A. Varfis, G.G. Wilkinson and J. Mégier, 1992, Land-cover discrimination in SPOT-HRV imagery using an artificial neural network - a 20-class experiment, *Int. J. Remote Sensing*, vol. 13, no. 5, 917-924.

Kawata, Y., S. Ueno and T. Kusaka, 1988, Radiometric correction for atmospheric and topographic effects on Landsat MSS images, *Int. J. Remote Sensing*, vol. 9, no. 4, 729-748.

Leprieur, C., J.M. Durand and J.L. Peyron, 1988, Influence of topography on forest reflectance using Landsat Thematic Mapper and digital terrain data, *Photogrammetric Engineering and Remote Sensing*, vol. 54, no. 4, 491-496.

Minnaert, M., 1941, The reciprocity principle in lunar photometry, *Astrophys. J.*, vol. 93, 403-411.

Proy, C., D. Tanré and P.Y. Deschamps, 1989, Evaluation of topographic effects in remotely sensed data, *Remote Sensing of Environment*, 30, 21-32.

Sobolev, V.V., 1963, *A treatise on radiative transfer*, (Van Nostrand: Princeton).

Tanré, D., M. Herman, P.Y. Deschamps and A. de Leffe, 1979, Atmospheric modelling of the background contribution upon space measurements of ground reflectance, including bi-directional properties, *Applied Optics*, 18, 3587-3594.

Tanré, D., C. Deroo, P. Duhaut, M. Herman and J.J. Morcrette, 1990, Description of a computer code to simulate the satellite signal in the solar spectrum: the 5S code, *Int. J. Remote Sensing*, vol. 11, no. 4, 659-668.

Temps, R.C. and K.L. Coulson, 1977, Solar radiation incident upon slopes of different orientation, *Solar Energy*, 19, 179-216.

Woodham, R.J. and M.H. Gray, 1987, An analytic method for radiometric correction of satellite multispectral scanner data, *IEEE Trans. on Geoscience and Remote Sensing*, vol. GE-22, no. 3, 258-271.

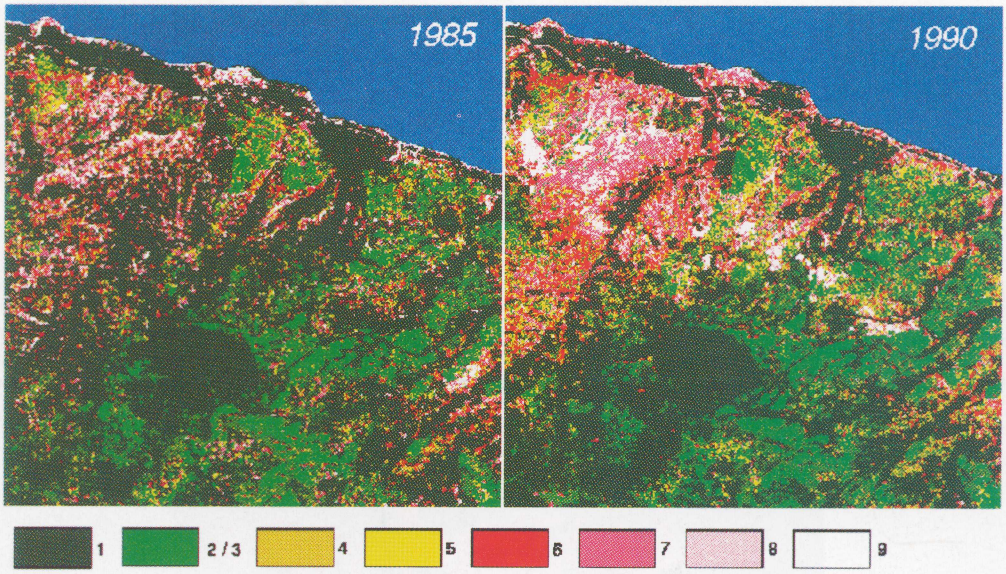

Figure 3. Peloponnese Greece: Comparison of land surface properties based upon a synoptic evaluation of Landsat-derived information layers on soil conditions and vegetation abundance. The numbers refer to 'desertification risk levels' in the sense of varying susceptibility to further degradation, ranking from 'stable' (1: vegetation cover more than 50% and soil condition index I) to 'irreversible degradation' (9: vegetation cover less than 20% and soil condition index IV) (Hill et al., page 57).

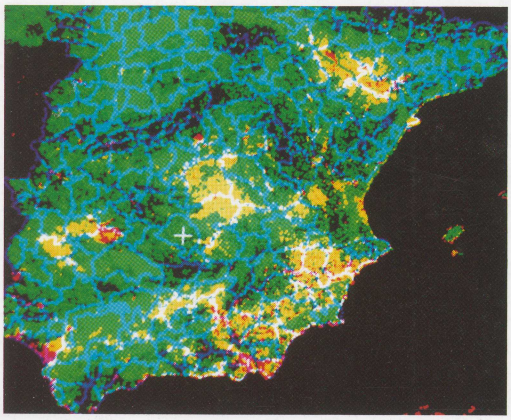

Photograph 1. 1993 drought zones (in yellow) (González Alonso et al., page 89).

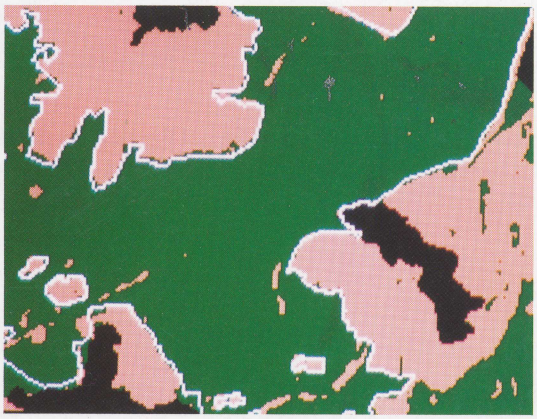

Figure 4. Classified radar image overlaped by the border of the forest land out of a forest map. Forest = green; agricultural land = sand; housing areas = black (Koch et al., page 94).

Figure 1. Digital elevation model of the Heiderscheid study area, illuminated according to the conditions during the Landsat satellite overpass from 21 September 1989 (top of page is north) (Hill et al., page 144).

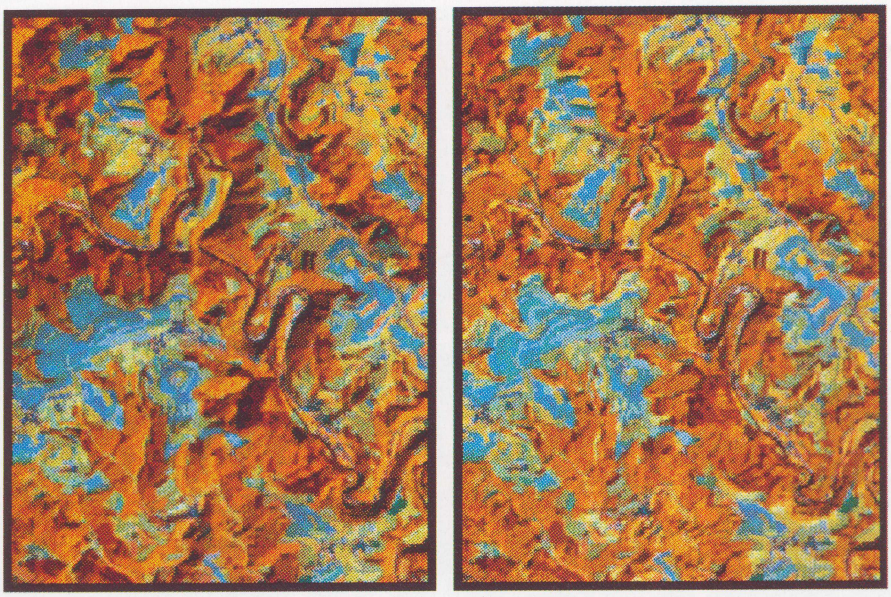

Figure 4. Colour composite of the Landsat image from 20 August 1989 (band combination is 4-5-3 in red-green-blue): atmospheric correction only (left) and atmospheric/topographic correction (right) (Hill et al., page 148).

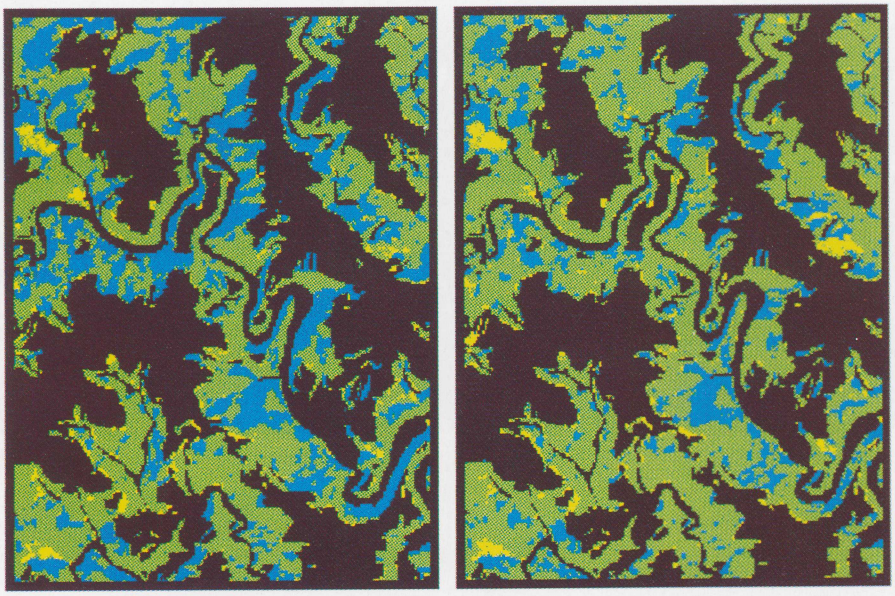

Figure 7. Comparison of forest mapping results for the Landsat TM scene from 20 August 1989, obtained with the neural network classifier before and after topographic corrections (blue – conifers, green – deciduous, yellow – storm damage) (Hill et al., page 150).

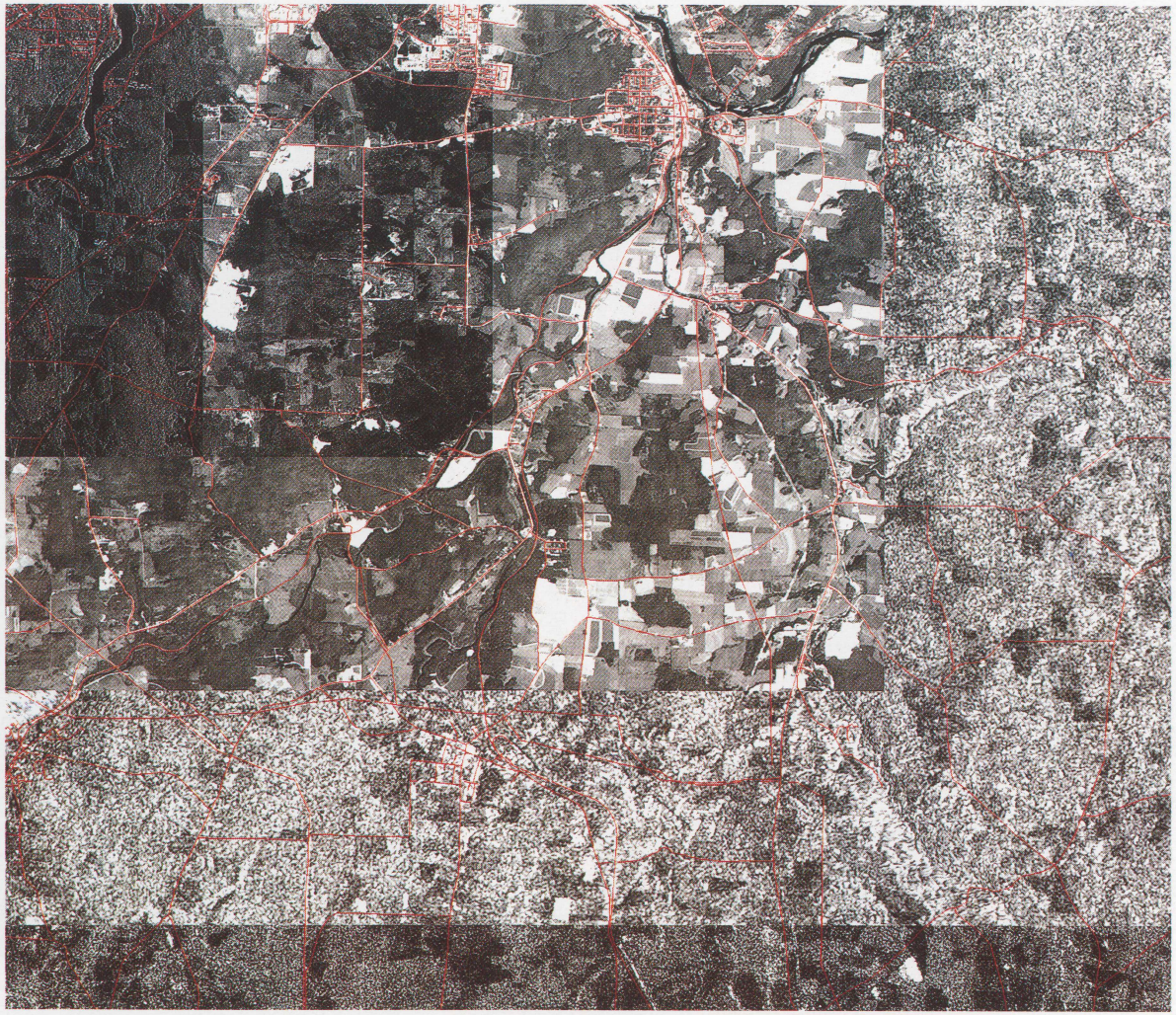

Figure 2. Enlargement of the ortho-mosaic (17 × 15 km; 10 m pixel size) (Toutin, page 169).